Supporting Information

Reactive Species and Reaction Pathways for the Oxidative Cleavage of 4-Octene and Oleic Acid with H_2O_2 over Tungsten Oxide Catalysts

Danim Yun,[1,2] E. Zeynep Ayla,[2] Daniel T. Bregante,[2] and David W. Flaherty[1,2]*

[1]DOE Center for Advanced Bioenergy and Bioproducts Innovation, University of Illinois at Urbana-Champaign
[2]Department of Chemical and Biomolecular Engineering, University of Illinois at Urbana-Champaign, Urbana, Illinois 61801

*Corresponding Author

Phone: (217) 244-2816

Email: dwflhrty@illinois.edu

S1. Stability of WO_x sites During Oxidative Cleavage of 4-C_8H_{16}

S1.1. Hot Filtration Test

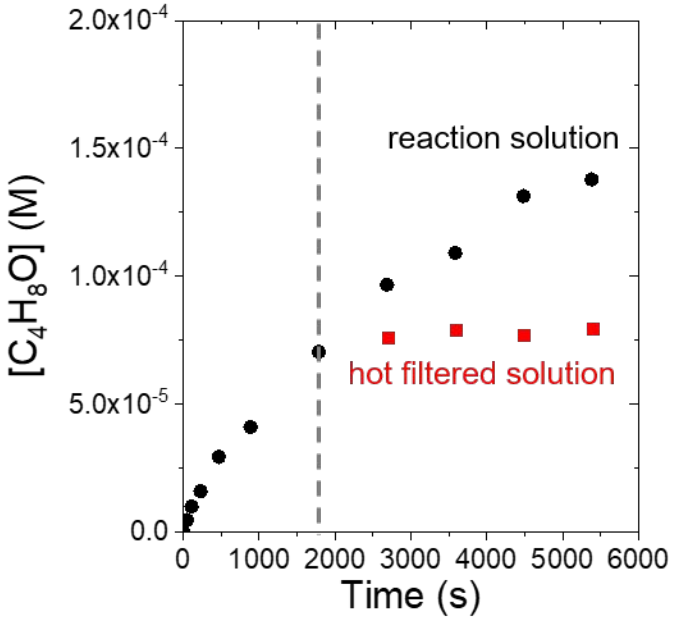

Figure S1. Butanal concentrations of (●) non-filtered reaction solution and (■) hot filtered solution as a function of reaction time (5 mM 4-C_8H_{16}, 0.1 M H_2O_2, 0.39 M H_2O in CH_3CN) over WO_x-Al_2O_3 at 333 K.

To determine if catalytically active forms of WO_x leach from the alumina support, we carried out hot filtration tests for WO_x-Al_2O_3 catalyst. Hot filtered solutions do not show any change in butanal concentration following filtration of catalyst (Figure S1). This result indicates that the active WO_x species do not leach from the alumina support.

S1.2. Regeneration of WO_x-Al_2O_3 catalyst

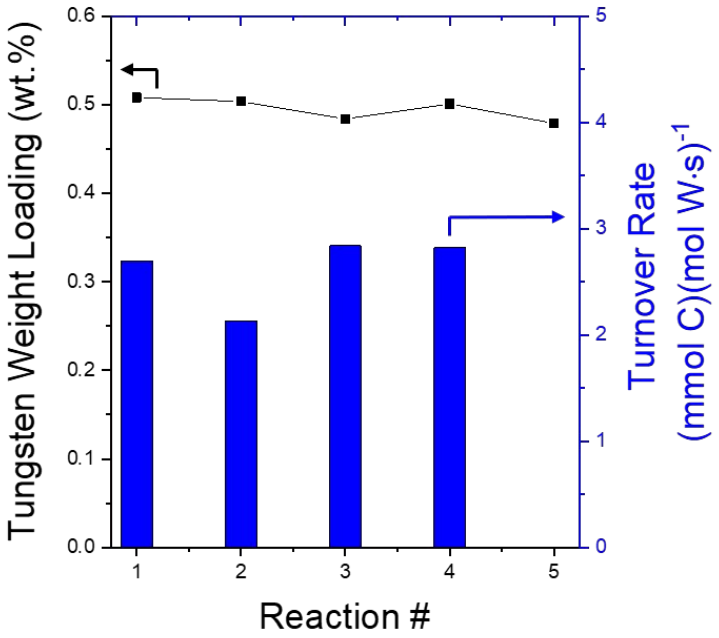

Figure S2. Tungsten weight loading of fresh and regenerated WO_x-Al_2O_3 catalysts and turnover rate for butanal formation during recycle test (5 mM 4-C_8H_{16}, 0.1 M H_2O_2, 0.39 M H_2O in CH_3CN) over WO_x-Al_2O_3 at 333 K.

To confirm the reusability of WO_x-Al_2O_3 catalyst, we conducted four subsequent batch reactions. EDXRF results show that the W content remained nearly constant at 0.50 ± 0.006% by weight throughout the course of the four reactions, and the turnover rates were consistently 2.6 ± 0.2 (mmol C)(mol W s)$^{-1}$ for all four reactions. This consistency demonstrates that the WO_x-Al_2O_3 catalysts are stable and regenerable.

S2. Additional Catalyst Characterization

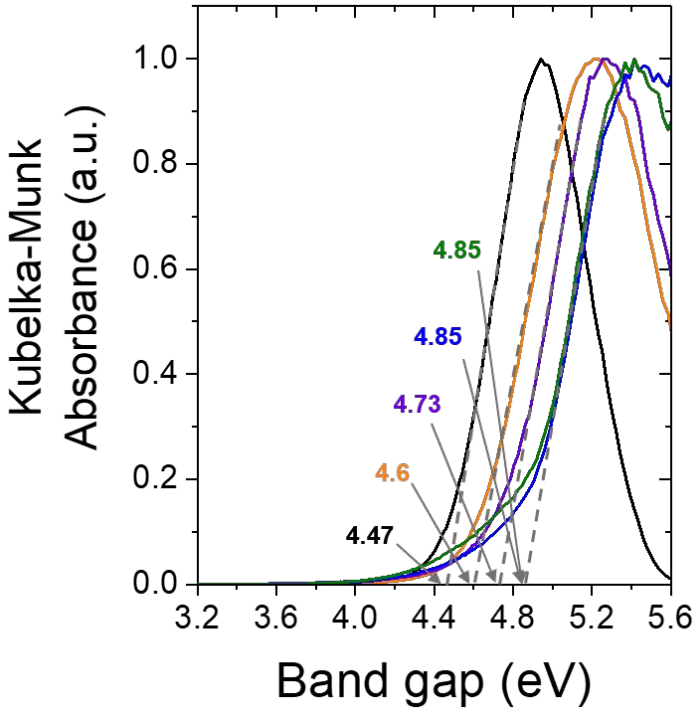

Figure S3. Tauc plots of the X-WO_x-Al_2O_3 (0.03 (—), 0.06 (—), 0.1 (—), 0.4 (—), and 0.9 (—) W-atoms per unit surface area) derived from DRUV-Vis spectra under ambient conditions

Figure S3 shows the Kubelka-Munk absorbances of X-WO_x-Al_2O_3 catalysts as a function of a photon energy (i.e., Tauc plot). X-WO_x-Al_2O_3 samples with surface coverages equal to or less than 0.06 W·nm^{-2} consistently exhibit a band gap energy of 4.85 eV. This suggests that materials with W-atom coverages below 0.06 W·nm^{-2} approach a constant distribution of WO_x complexes.

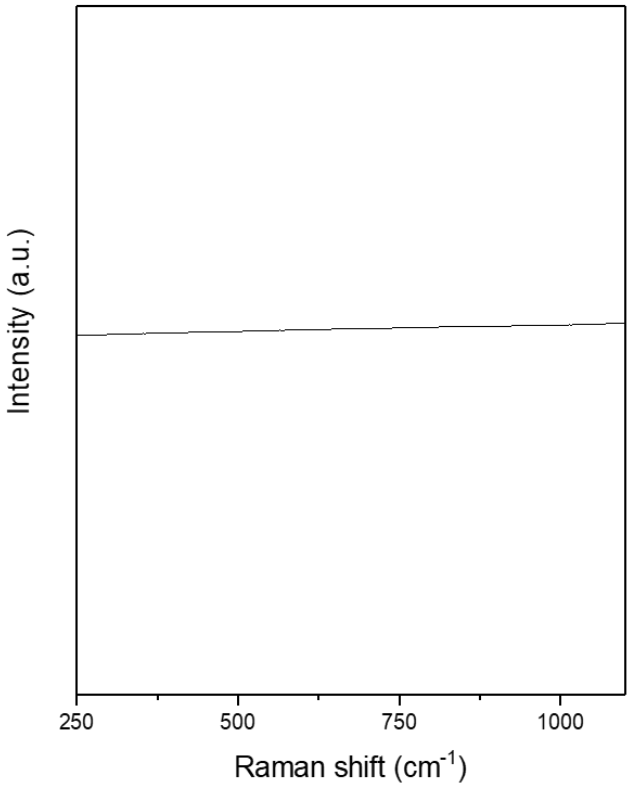

Figure S4. *Ex situ* Raman spectra taken with a 532 nm laser (1.6 mW·μm^{-2}) of γ-Al_2O_3 at 298 K

Figure S4 indicates γ-Al_2O_3 support does not give rise to any features visible in Raman.

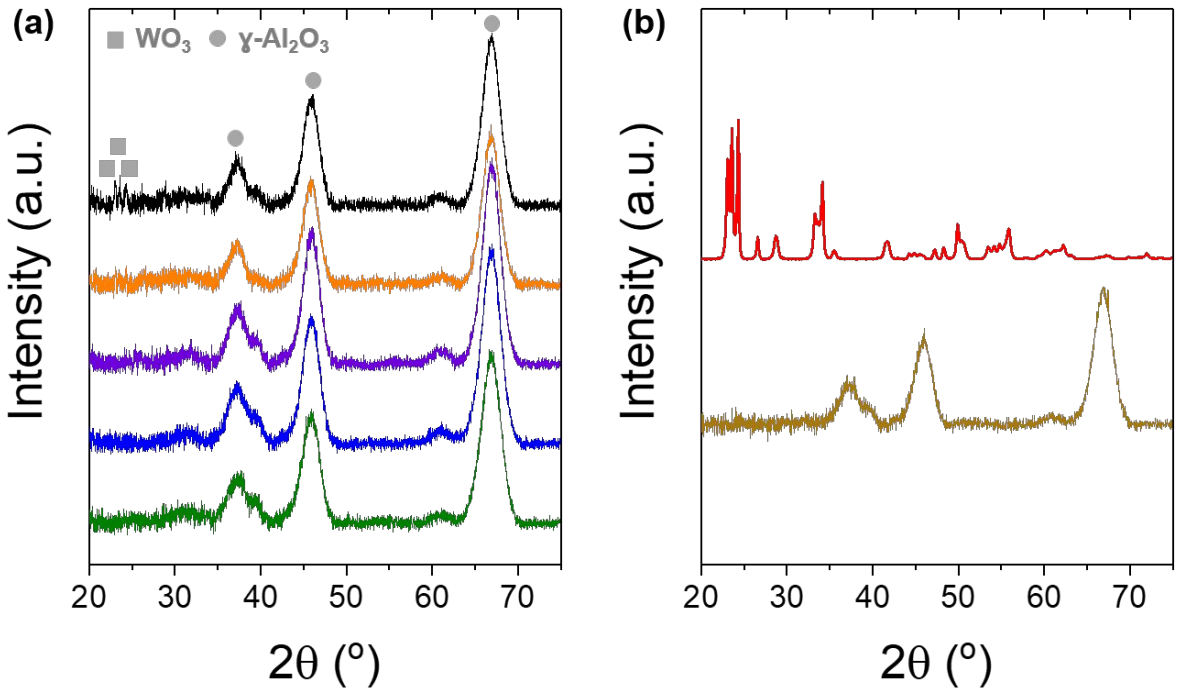

Figure S5. XRD patterns of (a) X-WO_x-Al_2O_3 (0.03 (—), 0.06 (—), 0.1 (—), 0.4 (—), and 0.9 (—) W-atoms per unit surface area, W·nm^{-2}) and (b) WO_3 NP (—), and γ-Al_2O_3 (—).

Figure S5 shows XRD patterns of WO_x-Al_2O_3 catalysts, WO_3 NP, and γ-Al_2O_3. The 0.9-WO_x-Al_2O_3 catalyst gives weak XRD peaks at 23, 23.6, and 24.4°, which correspond to crystalline WO_3 (JCPDS No. 83-950). This suggests that WO_x-Al_2O_3 catalysts with W-atoms surface coverages less than 0.9 W·nm^{-2} possess smaller and less ordered WO_x complexes.

S3. Reaction Pathways for the Oxidative Cleavage of 4-Octene and Oleic Acid over WO_3 and WO_x-Al_2O_3 catalysts

S3.1. Product Concentrations and Selectivities as Functions of Reaction Time for the Reactions of 4-Octene

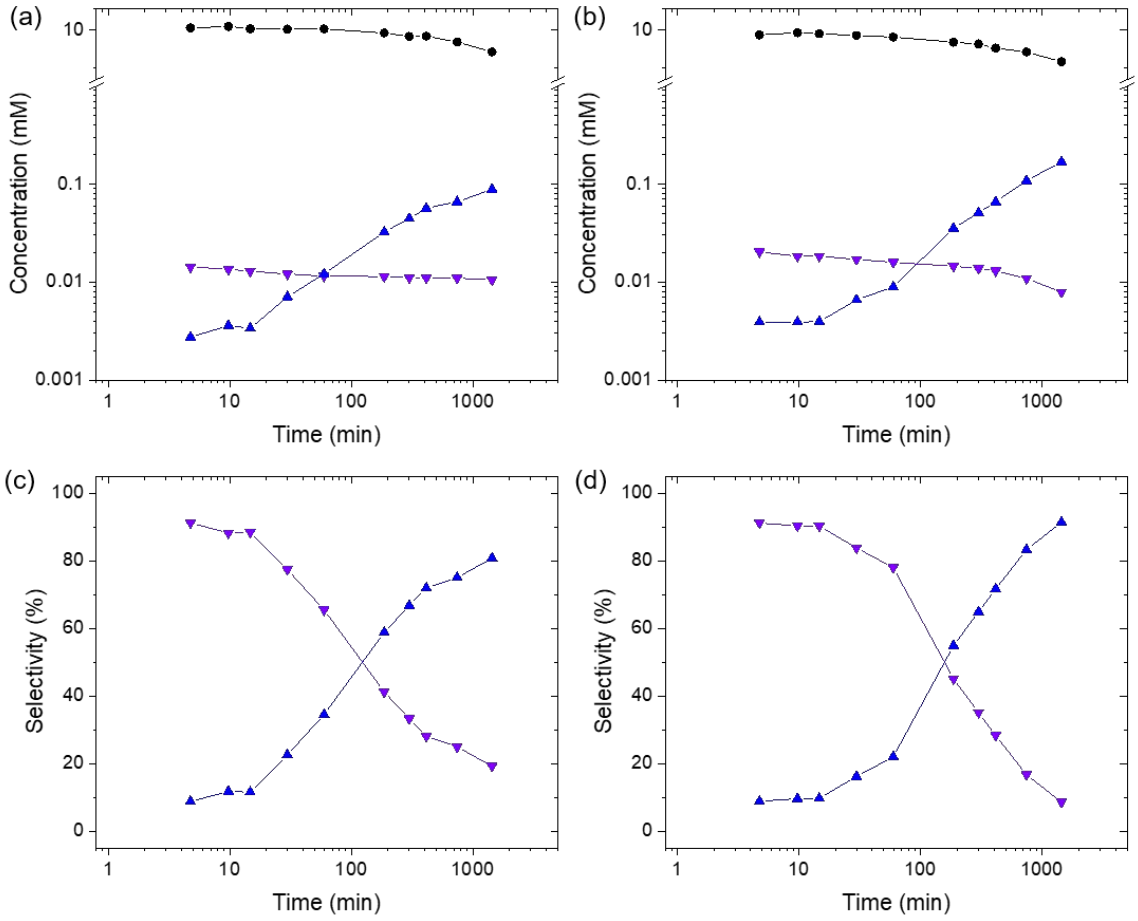

Figure S6. Concentrations of 4-octene (●), 4,5-epoxyoctane (▼), and butanal (▲) as a function of reaction time (10 mM 4-octene, 0.1 M H_2O_2, and 0.39 M H_2O in CH_3CN at 333 K) over (a) WO_3 and (b) WO_x-Al_2O_3, and selectivity towards 4,5-epoxyoctane (▼) and butanal (▲) as a function of reaction time (10 mM 4-octene, 0.1 M H_2O_2, and 0.39 M H_2O in CH_3CN at 333 K) over (c) WO_3 and (d) WO_x-Al_2O_3.

Figure S6 shows that selectivity towards 4,5-epoxyhexane is small (≤ 20% and 10% for WO_3 and WO_x-Al_2O_3, respectively) in comparison to butanal selectivities (~ 80% and ~90% for WO_3 and WO_x-Al_2O_3, respectively). These comparisons suggest that rates of steps 9 and 11 exceed that for

step 4 by a significantly amount (Scheme 3 in the masnuscript), which implies also an even greater difference between the associated rate constants (i.e., k_9, $k_{11} \gg k_4$).

S3.2. Turnover Rates for 4-Octene Consumption, Epoxide Production, and Aldehyde Production in 4-Octene Conversion

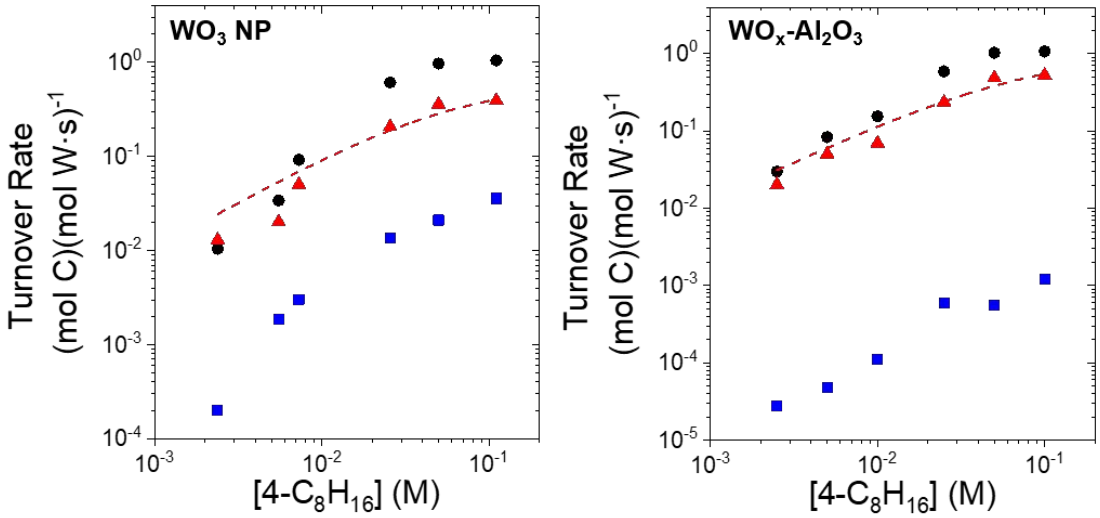

Figure S7. Turnover rates for 4-octene consumption (●), epoxide production (■), and butanal formation (▲) (0.1 M H_2O_2, and 0.39 M H_2O in CH_3CN at 333 K) as a function of [4-C_8H_{16}] over WO_3 and WO_x-Al_2O_3.

Table S1. Conversion and product selectivities over WO_3 and WO_x-Al_2O_3 in the oxidative cleavage of 4-C_8H_{16} with H_2O_2 (0.025-0.1 M 4-C_8H_{16}, 0.1 M H_2O_2, and 0.39 M H_2O in CH_3CN at 333 K)

Sample	Conversion (%)[a]	4,5-Epoxyoctane (%)[b]	Butanal (%)[b]
WO_3	< 3	≤ 5	95
WO_x-Al_2O_3	< 4	≤ 5	95

[a] alkene conversion (%) = $\frac{mole\ of\ alkene\ reacted}{mole\ of\ alkene\ fed} \times 100$

[b] selectivity (%) = $\frac{mole\ of\ C\ in\ product}{mole\ of\ C\ in\ all\ products} \times 100$

Figure S7 shows turnover rates for 4-octene consumption, epoxide formation, and butanal formation (0.1 M H_2O_2, and 0.39 M H_2O in CH_3CN at 333 K) over WO_3 and WO_x-Al_2O_3. Over both catalysts, turnover rates for products formation ((mol C) (mol W s)$^{-1}$) match rates for 4-octene consumption within 30% at conditions and low conversions used here, and selectivity for butanal is ≥ 95%. Therefore, we used butanal formation rates to report oxidative cleavage rates.

S3.3. Product Concentrations and Selectivities as Functions of Reaction Time for the Reactions of Oleic Acid

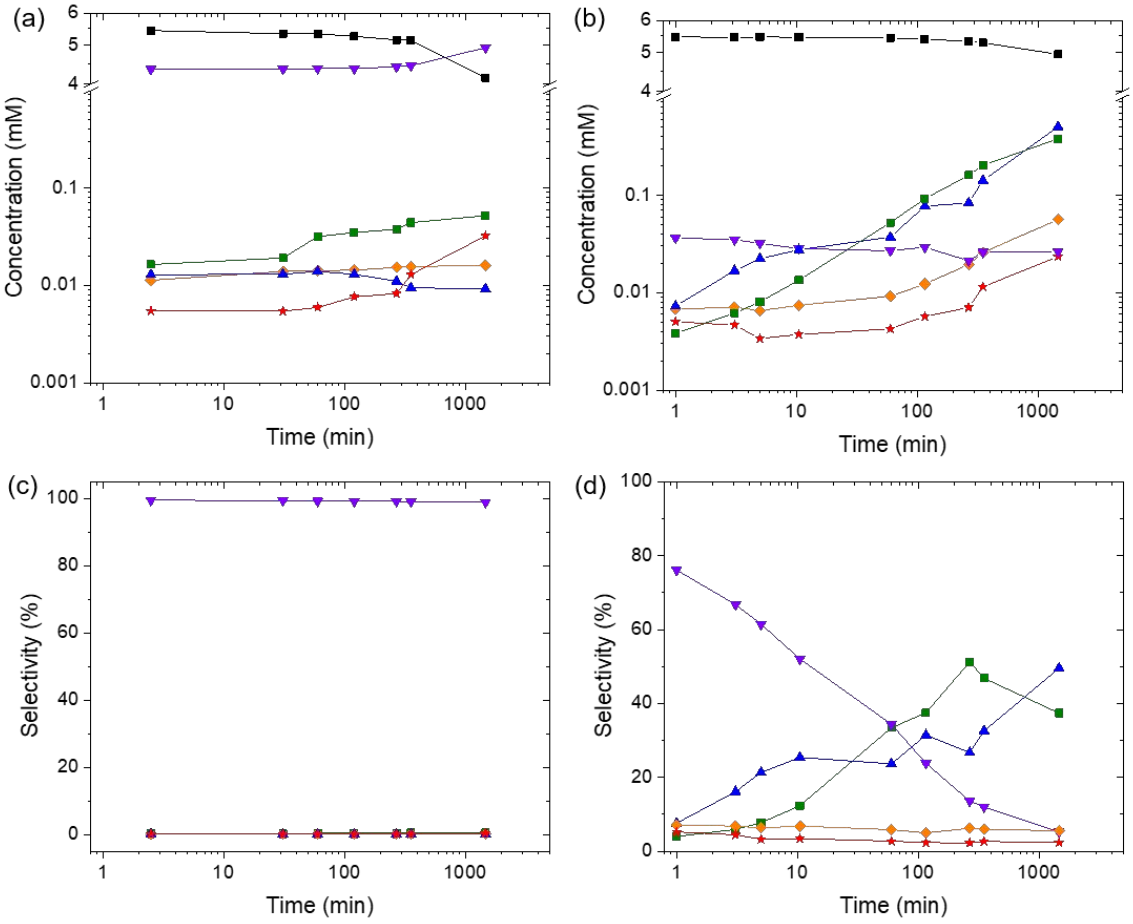

Figure S8. Concentrations of oleic acid (●), 8-(3-octyloxiran-2-yl)octanoic acid (▼), nonanal (■), azelaaldehydic acid (▲), nonanoic acid (◆), and azelaic acid (★) as a function of reaction time (5.5 mM OA, 0.5 M H_2O_2, and 1.98 M H_2O in CH_3CN at 343 K) over (a) WO_3 and (b) WO_x-Al_2O_3, and selectivity towards 8-(3-octyloxiran-2-yl)octanoic acid (▼), nonanal (■), azelaaldehydic acid (▲), nonanoic acid (◆), and azelaic acid (★) as a function of reaction time (5.5 mM OA, 0.5 M H_2O_2, and 1.98 M H_2O in CH_3CN at 343 K) over (c) WO_3 and (d) WO_x-Al_2O_3

Figure S8 shows that the selectivity towards epoxide is ~99 % over WO_3, and therefore, we measured turnover rates for epoxidation for WO_3 catalyst. On the other hand, selectivity towards oxidative cleavage products (e.g. aldehydes and acids) are gradually greater (> 80% over 2 h) than epoxide selectivity (≤ 20% over 2 h) over WO_x-Al_2O_3. Therefore, we measured turnover rates for oxidative cleavage products formation for the supported catalyst.

S3.4. Turnover Rates for Oleic Acid Consumption, Epoxide Production, and Aldehyde and Acid Production in Oleic Acid Conversion

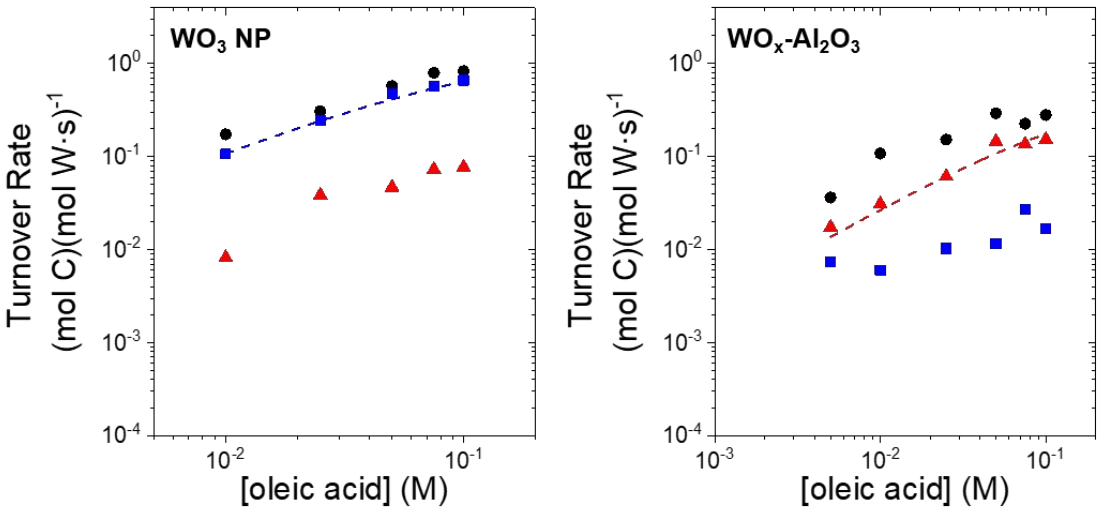

Figure S9. Turnover rates for oleic acid consumption (●), epoxide production (■), and nonanal, nonanoic acid, azelaaldehydic acid and azelaic acid formations (▲) (0.5 M H_2O_2, and 1.98 M H_2O in CH_3CN at 343 K) as a function of [oleic acid] over WO_3 and WO_x-Al_2O_3.

Table S2. Conversion and product selectivities over WO_3 and WO_x-Al_2O_3 in the oxidative cleavage of oleic acid with H_2O_2 (0.01-0.1 M oleic acid, 0.5 M H_2O_2, and 1.98 M H_2O in CH_3CN at 343 K)

Sample	Conversion (%)[a]	Epoxide (%)[b]	Nonanal (%)[b]	Nonanoic acid (%)[b]	Azelaaldehydic acid (%)[b]	Azelaic acid (%)[b]
WO_3	< 6	98	0.6	0.4	0.5	0.5
WO_x-Al_2O_3	< 2	20	35	5	15	25

[a]alkene conversion (%) = $\frac{mole\ of\ alkene\ reacted}{mole\ of\ alkene\ fed} \times 100$

[b]selectivity (%) = $\frac{mole\ of\ C\ in\ product}{mole\ of\ C\ in\ all\ products} \times 100$

Figure S9 shows turnover rates for oleic acid consumption, epoxide formation, and oxidative cleavage products formation over WO_3 and WO_x-Al_2O_3 at 343 K. The turnover rates of epoxide formation and oxidative cleavage products formation over WO_3 and WO_x-Al_2O_3, respectively, match rates for oleic acid conversion (80% for WO_3 and 60% for WO_x-Al_2O_3). Therefore, epoxide production and oxidative cleavage product formations provide an accurate basis to report oleic acid consumption over WO_3 and WO_x-Al_2O_3, respectively.

S4. Role of H_2O on Oxidative Cleavage of 4-C_8H_{16} and Oleic Acid

S4.1. Turnover Rates for Butanal Formation as a Function of Water Concentration

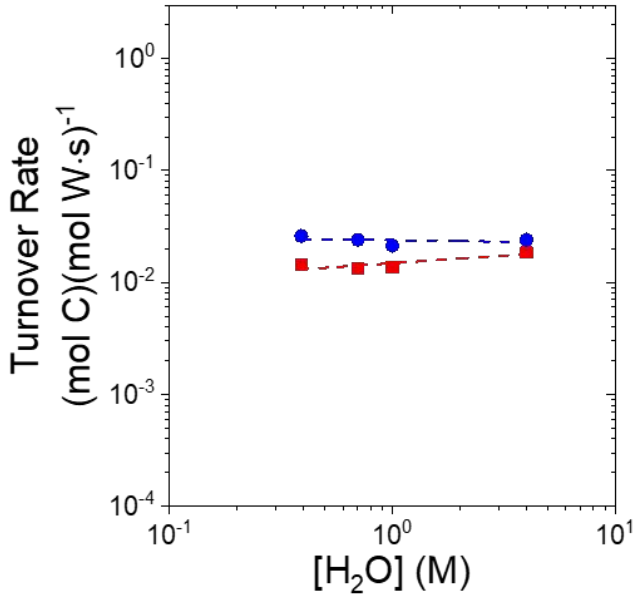

Figure S10. Turnover rates for oxidative cleavage of 4-octene (butanal formation) as a function of [H_2O] for WO_3 (■, 2.5 mM 4-C_8H_{16}, 0.1 M H_2O_2) and WO_x-Al_2O_3 (●, 2.5 mM 4-C_8H_{16}, 0.1 M H_2O_2) at 333 K.

Figure S10 shows turnover rates for butanal formation do not depend on [H_2O] over both WO_3 and WO_x-Al_2O_3 catalysts, which suggests that any interactions between H_2O molecules and H_2O_2-derived reactive intermediates (i.e., W-(η^2-O_2) and W-OOH) or transition states remain constant across this range of conditions (0.39 to 4.0 M H_2O).

S4.2. Role of H_2O and H_2O_2 in Oxidative Cleavage of Oleic Acid

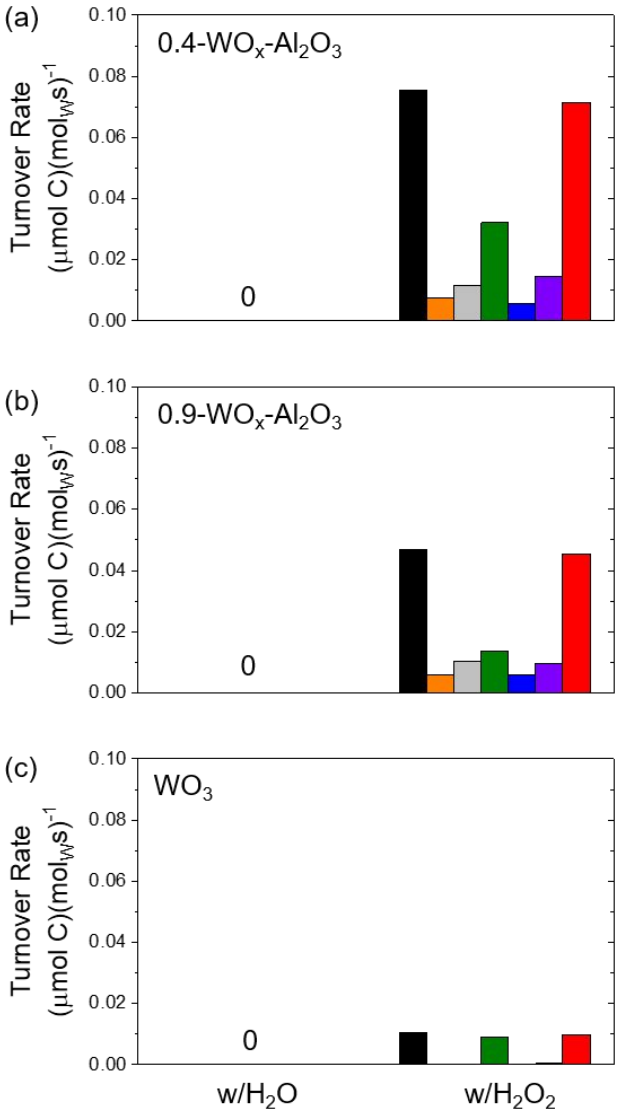

Figure S11. Turnover rates for the consumption of C in oleic acid(■), the formations of C in 8-(3-octyloxiran-2-yl)octanoic acid (■), nonanal (■), nonanoic acid (■), 9-oxononanoic acid (■), azelaic acid (■), all products (■) with H_2O (0.05 M oleic acid, 1.98 M H_2O) or H_2O_2 (0.05 M oleic acid, 0.5 M H_2O_2, 1.98 M H_2O) on 0.4 W·nm^{-2}, 0.9 W·nm^{-2}, and WO_3 at 343 K

Figure S11 suggests H_2O_2 is required for oxidative cleavage of oleic acid, and this reaction does not proceed in the absence of H_2O_2.

S5. Derivation of the Rate Expression

S5.1 Pseudo Steady State Hypothesis Applied to W-(η^2-O_2) and W-OOH Intermediates

We can assume that the concentration of a specific reactive species is not changing as a function of time during a reaction by using the pseudo steady state hypothesis (PSSH). Application of the PSSH to W-(η^2-O_2) and W-OOH intermediates of tungsten oxide catalysts in section 3.5 yields:

$$\frac{d[W-OO]}{dt} \approx 0 = k_3[H_2O_2*] - k_4[C_8H_{16}][W-OO] - k_6[H_2O_2][W-OO] \quad \text{(S1)}$$

where k_x represents the rate constant for step x, [*W-OO*] is the number of W-(η^2-O_2) and W-OOH, [H_2O_2*] is the number of H_2O_2 molecules bound to active sites, and all other species within brackets ([]) are the corresponding liquid-phase concentrations. When H_2O_2 adsorption is assumed to be quasi-equilibrated (step 2, Scheme 3), Equation S1 can be rearranged to yield:

$$[W-OO] = \frac{k_3K_2[H_2O_2][*]}{k_4[C_8H_{16}] + k_6[H_2O_2]} \quad \text{(S2)}$$

where [*] is the number of unoccupied (or solvent-covered) active sites. Equation S2 is then combined with Equation 3 (main text) to yield Equation 4 from the main text.

S5.2 Derivation of the Rate Expression for H_2O_2 Decomposition

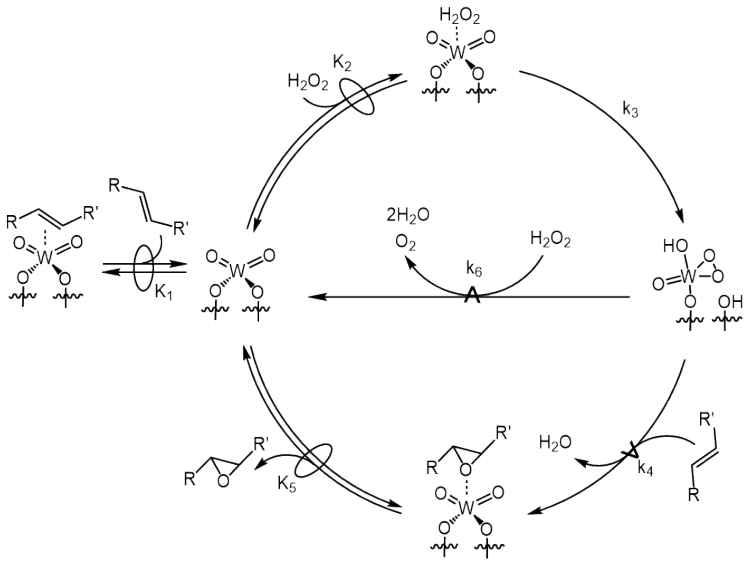

Scheme S2. Proposed elementary steps for epoxidation of alkene and H_2O_2 decomposition over tungsten oxide catalysts. The ⇄ symbol denotes a quasi-equilibrated step and the ⇢ symbol signifies a kinetically relevant step.

Scheme S2 shows a series of elementary steps that are consistent with the rate measurements for 4-C_8H_{16} conversion with H_2O_2 (Figure 6). This catalytic cycle involves the quasi-equilibrated adsorption of 4-C_8H_{16} (step 1) and H_2O_2 (step 2), and the irreversible activation of adsorbed H_2O_2 (step 3) to form W-(η^2-O_2) intermediates. W-(η^2-O_2) reacts with 4-C_8H_{16} (step 4) to form epoxide or with H_2O_2 to form decomposition products (e.g., water and oxygen) (step 6). The reaction between W-(η^2-O_2) and H_2O_2 is kinetically relevant, which leads to rate for H_2O_2 decomposition (r_D)

$$r_D = k_6\,[H_2O_2][\mathrm{W}-OO] \qquad \text{(S3)}$$

where k_x represents the rate constant for step x in Scheme S2, [W-OO] is the number of W-(η^2-O_2) and W-OOH, and [H_2O_2] is liquid-phase concentrations of H_2O_2. The application of pseudo-steady state hypothesis on [W-OO] leads to equation S3 to be restated as:

$$\frac{r_D}{[L]} = \frac{\frac{k_3 k_6 K_2 [H_2O_2]^2}{k_4[4-C_8H_{16}] + k_6[H_2O_2]}}{1 + K_1[4-C_8H_{16}] + K_2[H_2O_2] + \frac{k_3 K_2 [H_2O_2]}{k_4[4-C_8H_{16}] + k_6[H_2O_2]} + \frac{[4{,}5-C_8H_{16}O]}{K_5}} \qquad \text{(S4)}$$

where [L] is the total number of active sites and K_x is the equilibrium constant for step x in Scheme S2. The five terms in the denominator signify the numbers of sites that are occupied by CH_3CN, 4-C_8H_{16}, H_2O_2, W-(η^2-O_2) and W-OOH, and 4,5-$C_8H_{16}O$, respectively.

When the W-(η^2-O_2) and W-OOH species become the most abundant reactive intermediate (MARI), the complete form of rate expression (equation S4) takes the common form:

$$\frac{r_D}{[L]} = k_6[H_2O_2] \qquad \text{(S5)}$$

This simpler form well matches with experimental results shown in Figure S12 that show turnover rates for H_2O_2 decomposition over Al_2O_3 and WO_3-Al_2O_3 increase linearly with the H_2O_2 concentration at conditions where the turnover rates for 4-octene consumption are proportional to [4-C_8H_{16}] (Figure 6a), and invariant with [H_2O_2] (Figure 6b), because the MARI are W-(η^2-O_2) and W-OOH species intermediates.

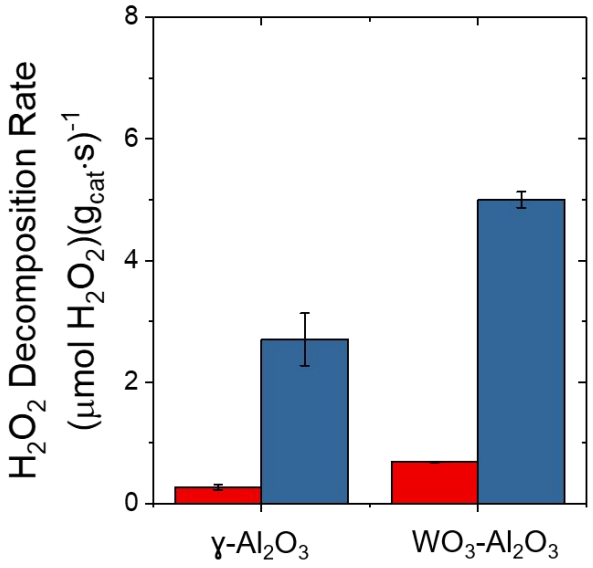

Figure S12. H_2O_2 decomposition rates over γ-Al_2O_3 and WO_x-Al_2O_3 (■, 10 mM H_2O_2, 39 mM H_2O; ■, 0.1 M H_2O_2, 0.39 M H_2O) at 333 K

From these expressions, the ratio of the rates for epoxidation to decomposition can be represented by the following equation:

$$\frac{r_E}{r_D} = \frac{k_4[4-C_8H_{16}]}{k_6[H_2O_2]} \qquad \text{(S6)}$$

where equation S6 indicates the selectivity for the consumption of H_2O_2 by epoxidation (step 4) or by H_2O_2 decomposition (step 6) depends on the concentrations of 4-C_8H_{16} and H_2O_2. Moreover, this rate ratio increases in proportion to the ratio of the reactant concentrations ([4-C_8H_{16}]/ [H_2O_2]).

S6. Activation Enthalpies and Entropies for Oxidative Cleavage of 4-Octene and 1,2-Epoxyoctane Heats of Adsorption

S6.1. Measurement of Activation Enthalpies and Entropies

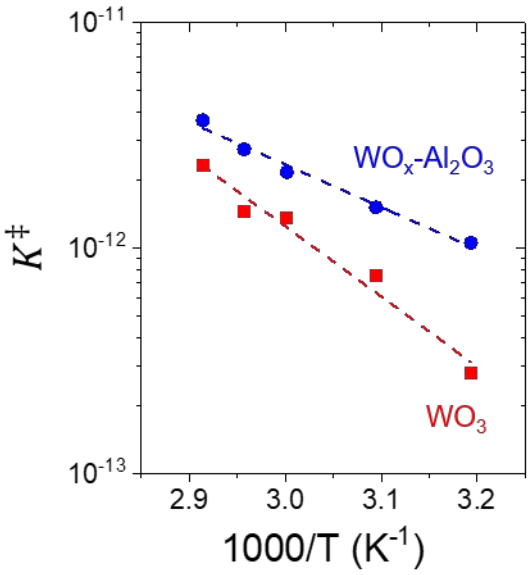

Figure S13. Transition state equilibrium constants for oxidative cleavage of 4-octene as a function of inverse temperature on WO_x-Al_2O_3 (■, 0.01 M 4-C_8H_{16}, 0.1 M H_2O_2, 0.39 M H_2O) and WO_3 (●, 0.01 M 4-C_8H_{16}, 0.1 M H_2O_2, 0.39 M H_2O) in CH_3CN. Dashed lines represent fits to the Eyring equation whose slopes are proportional to $\Delta H^{\ddagger}$.

The apparent activation enthalpy and entropy can be determined by regression of measured $K_{OC}^{\ddagger}$ as a function of inverse temperature, because $K_{OC}^{\ddagger}$ can be expressed in terms of $\Delta H_{OC}{}^{\ddagger}$ and $\Delta S_{OC}{}^{\ddagger}$ as follow:

$$K_{OC}^{\ddagger} = e^{\left(\frac{-\Delta H_{OC}{}^{\ddagger}}{RT} + \frac{\Delta S_{OC}{}^{\ddagger}}{R}\right)} \qquad \text{(S7)}$$

where R is the ideal gas constant. $\Delta H_{OC}{}^{\ddagger}$ and $\Delta S_{OC}{}^{\ddagger}$ values for WO_3 and WO_x-Al_2O_3 catalysts were determined from Figure S13. $\Delta H_{OC}{}^{\ddagger}$ over WO_x-Al_2O_3 (36 ± 3 kJ·mol^{-1}) is ~ 24 kJ·mol^{-1} lower than over WO_3 (60 ± 6 kJ·mol^{-1}), which suggests that differences in the electronic structure of catalytically W-active sites supported on γ-Al_2O_3 enthalpically favor epoxidation and subsequent oxidative cleavage of 4-octene by a significant margin. $\Delta S_{OC}{}^{\ddagger}$ values over WO_3 and WO_x-Al_2O_3 catalysts were -49 ±18 and -114 ± 8 kJ·mol^{-1}, respectively, which suggest the favorable binding enthalpy of transition state has to overcome an unfavorable loss of entropy.

In the oxidative cleavage of 4-C_8H_{16} with H_2O_2 over WO_x sites, the entropy losses must result from the coordination of 4-C_8H_{16} to the reactive W-(η^2-O_2) species to form the epoxidation transition states. There are at least two plausible reasons this process may result in a greater entropy loss over WO_x-Al_2O_3 than on WO_3 First, the active sites of WO_x-Al_2O_3 possess greater Lewis acid strength than those on WO_3 (Figure 7, Table 2), which leads to more tightly bound transition states upon WO_x-Al_2O_3. Second, the hydroxyl groups and pore structure of the alumina support may influence the composition and ordering of the solvent molecules about the active sites, which would lead to differences in excess thermodynamic contributions that differ between the two materials. Other factors may also contribute, however, the specific cause of the large difference in $\Delta S_{OC}^{\ddagger}$ (~ 65 J mol^{-1} K^{-1}) is not clear at this time. The compensation between $\Delta H_{OC}^{\ddagger}$ and $\Delta S_{OC}^{\ddagger}$ gives rise to turnover rates that differ by only 75% between WO_3 and WO_x-Al_2O_3 catalysts at 333 K, despite values of $\Delta H_{OC}^{\ddagger}$ over WO_x-Al_2O_3 (36 ± 3 kJ·mol^{-1}) that are ~ 24 kJ·mol^{-1} lower than over WO_3 (60 ± 6 kJ·mol^{-1}).

S6.2. Changes in Enthalpy for the Formation of the Transition State and the Epoxide Adsorption to the Tungstates Active Site

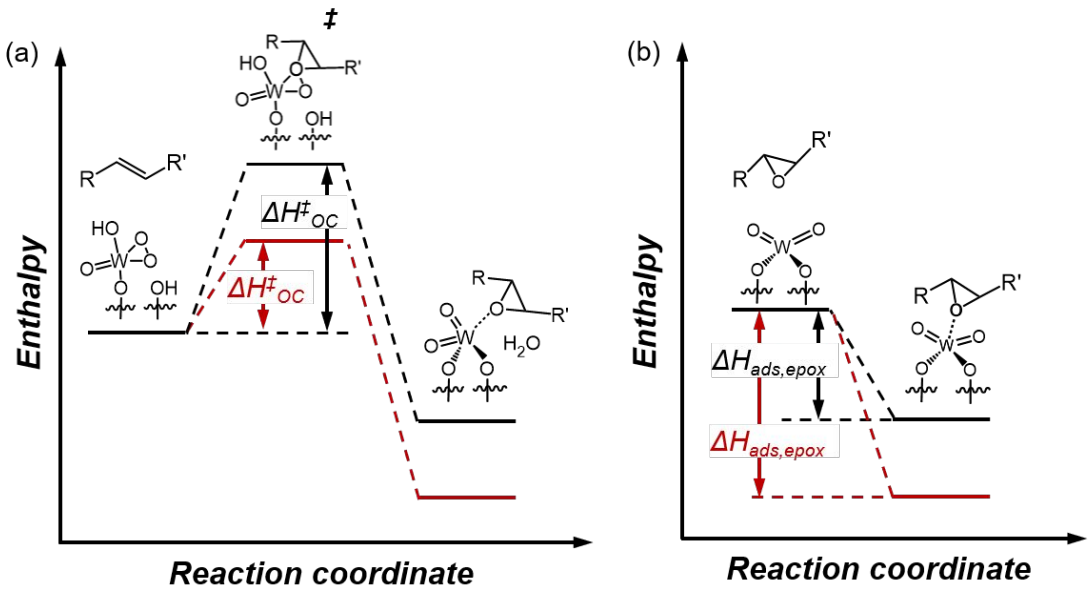

Scheme S2. Changes in enthalpy that correspond to (a) the formation of the transition state for rate-determining step of oxidative cleavage ($\Delta H^{\ddagger}_{OC}$) and (b) the adsorption of 1,2-epoxyoctane to the W site of the WO_x-Al_2O_3 (—) and WO_3 (—) catalysts.

Scheme S2 illustrates enthalpy changes corresponding to the formation of the transition state for epoxidation, which is the kinetically relevant transition state for oxidative cleavage of 4-octene, and the adsorption of 1,2-epoxyoctane onto the W site. Noticeably, the transition state structure (Scheme S1a) closely resemble the structural changes induced by adsorption of the 1,2-epoxyoctane (Scheme S1b).